Journal of Crystal Growth 312 (2010) 2363–2368

Contents lists available at ScienceDirect

Journal of Crystal Growth

journal homepage: www.elsevier.com/locate/jcrysgro

Microstructure evolution of lime putty upon aging

Giuseppe Mascolo [a], Maria Cristina Mascolo [a], Alessandro Vitale [a], Ottavio Marino [b,*]

[a] Dipartimento di Meccanica, Strutture, Ambiente e Territorio, Laboratorio Materiali, Università di Cassino, Italy
[b] Dipartimento di Ingegneria dei Materiali e della Produzione, Università di Napoli Federico II, Italy

ARTICLE INFO

Article history:
Received 27 January 2010
Received in revised form
21 April 2010
Accepted 16 May 2010
Communicated by S. Uda
Available online 24 May 2010

Keywords:
A1. Crystal morphology
A1. Growth models
A2. Growth from solution
B1. Calcium hydroxide

ABSTRACT

The microstructure evolution of lime putty upon aging was investigated by slaking quicklime (CaO) with an excess of water for 3, 12, 24, 36, 48 and 66 months.

The as-obtained lime putties were characterized in the water retention and in the particle size distribution using the static laser scattering (SLS). The same lime putties, dehydrated by lyophilization, were also investigated in the pore size distribution by mercury intrusion porosimetry, in the surface area by the BET method and, finally, in particle morphology by scanning electron microscopy (SEM).

The effect of the extended exposure of quicklime to water confirms a shape change from prismatic crystals of portlandite, $Ca(OH)_2$, into platelike ones. Simultaneously a growth of larger hexagonal crystals at the expense of the smallest ones (Ostwald ripening) favours a secondary precipitation of submicrometer platelike crystals of portlandite. The shape change and the broader particles size distribution of portlandite crystals upon aging seem to contribute to a better plasticity of lime putty.

1. Introduction

Over the last decades, there is a return of lime binders for plasters and mortars as the materials of choice for the conservation of historical and architectural structures [1–5]. To some extent, lime replaces the use of Portland cements owing to chemical and physical incompatibility between materials of historical buildings and relatively modern cement-based materials [6]. On the other hand Portland cements determine also a release of soluble salts promoting damage through crystallization [7].

Among lime binders, lime putty has been a building material since 8000 BC and is still one of the most important components in the formulation of plasters and mortars. It is produced by slaking quicklime (CaO) with an excess of water for extended periods of time until a creamy texture is produced. Extended aging of lime putty has been recognized for centuries as a means to improve the quality of hydrated lime as a binder in lime-based mortar and plasters [8,9]. Romans forbade the use of any lime putty that was less than three years old. The effect of extended exposure of lime putty to water indicates that portlandite crystals, $Ca(OH)_2$, undergo both an important size reduction and a shape change from prism to platelike crystals agglomerated as aggregates [10,11].

A model for portlandite evolution is based on the fact that submicrometer platelike crystal sizes originate from large pre-existing prismatic crystals due to the preferential dissolution of prism faces with a consequent heterogeneous secondary crystallization [11]. The sole crystal sizes reduction over time contrasts with the "Ostwald ripening" concerning the growth of the larger crystals at the expense of the smallest ones [12]. A conflicting model suggested, in fact, the formation of large platelike crystals [2].

The crystal size reduction of portlandite upon aging and the corresponding formation of platelike crystals account for the quality improvement in terms of plasticity and workability of lime-putty-based mortars [13–17].

In order to investigate thoroughly the discrepancy between the crystal size reduction and the growth of large crystals of portlandite, the microstructure evolution of a lime putty with slaking periods of 3 months up to 66 months has been investigated.

2. Experimental procedure

Six samples of lime putty aged under an excess of water for 3, 12, 24, 36, 48 and 66 months (thereafter denoted LP*X*, where *X* is the number of aging months) were tested.

The chemical composition of the quicklime precursor of lime putty is reported in Table 1. Each sample was taken from the inside of the lime putty avoiding contact with the supernatant water. The water retention content of the samples was determined by thermal treatments in an air oven at 110 °C up to constant weight. The results refer to measurements performed

* Corresponding author.
E-mail address: otmarino@unina.it (O. Marino).

0022-0248/$ - see front matter © 2010 Elsevier B.V. All rights reserved.
doi:10.1016/j.jcrysgro.2010.05.020

Table 1
Chemical composition (wt %) of the quicklime precursor.

CaO	MgO	Na_2O	K_2O	Fe_2O_3	Al_2O_3	SiO_2	CO_2	H_2O	SO_3
94.3	1.8	0.2	< 0.001	< 0.03	< 0.001	< 0.002	2.5	0.6	0.3

on three specimens for each sample. The amounts of portlandite, brucite and calcite were determined by thermogravimetric analysis (TGA) on samples dehydrated by lyophilization using a Lio Cinquepascal apparatus (Milan, Italy). The weight losses of the corresponding thermal decompositions of $Mg(OH)_2$ (brucite) into MgO, $Ca(OH)_2$ into CaO and $CaCO_3$ (calcite) into CaO were measured using a Netzsch model 409 thermoanalyzer (Selb-Bavaria, Germany), with α-Al_2O_3 as reference and a 10 °C/min heating rate.

The specific surface area of the dehydrated powders was measured by nitrogen adsorption according to the BET method using a Gemini instrument from Micromeritics (Norcross, GA, USA). The particle morphology was investigated by scanning electron microscopy (SEM), using a Philips microscope (XL series, Almelo, The Netherlands). The pore size distribution of the dehydrated powders was determined by mercury intrusion porosimetry using an instrument autoPore III of Micromeritics (Norcross, GA, USA). The particle size distribution of the as-obtained samples was investigated by static laser scattering using a Mastersizer 2000 granulometer of Malvern (Worcestershire, UK). In order to reduce aggregation phenomena of the as-obtained samples, they were previously suspended in an excess of alcohol and then submitted to ultrasonic treatment.

3. Results

Fig. 1 shows the differential scanning calorimetry (DSC) and the thermogravimetric analysis (TGA) of the 36-month-old aged lime putty previously dehydrated by lyophilization. Three DSC peaks can be observed, the small one at 363 °C concerns the $Mg(OH)_2$ decomposition, while the peaks at 475 °C and 684 °C to the decompositions of $Ca(OH)_2$ and $CaCO_3$, respectively. From the corresponding weight losses, the amounts of brucite, portlandite and calcite have been calculated and reported in Table 2 along with the results of the lime putties slaked for different periods. The brucite content, derived from the MgO impurity of the starting quicklime (Table 1), increases as the slaking period increases, reaching a constant value after 36 months. The complete conversion of the main component CaO of the quicklime into portlandite requires a shorter hydration time but higher than 12 months. The effect of the incomplete hydration of CaO and MgO justifies a total mineralogical composition lower than 100% for the LP3, LP12, LP24, LP36 samples. In conclusion, the complete hydration of CaO and MgO requires slaking times of 24 and 36 months, respectively. TGA analysis also reveals that all the lime putties are characterized by the presence of $CaCO_3$ with an average content of 10 wt%.

A same cumulative intruded volume of mercury (~1.7 mL/mg), measured by mercury porosimetry, resulted in all the lime putties with the exception of the 66-month-slaked one characterized by a slightly higher value (1.8 mL/mg). The detected wide range of the pore sizes distributions, changing between 0.1 and 200 μm, involves a wide range of particle size distributions. For clarity, only the pore size distributions of the lime putties slaked for 3, 24 and 66 months have been reported in Fig. 2. The shortest-month-slaking lime putty is characterized by the predominant presence of pore diameters in the range 10–40 μm, the 24-month-slaking one predominant pore diameters in the range 100–200 μm, whereas longest-month-slaking lime putty reveals a conspicuous increment of the pore diameters in the range 2–8 μm. The wide range in the pore size distributions of all the samples might be partly ascribed to the drying effect on the aggregation of the particles; however a corresponding heterogeneous particles size distribution must be expected for the differently aged lime putties.

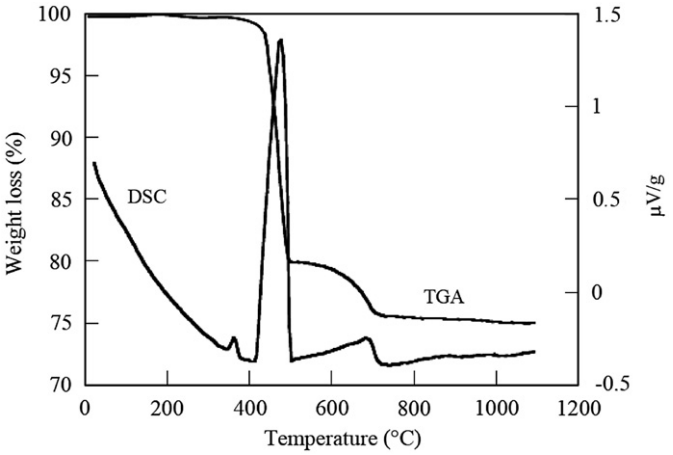

Fig. 1. Differential scanning calorimetry (DSC) and thermo-gravimetric analysis. (TGA) curves of 36 month aged lime putty previously dehydrated by lyophilisation.

Table 2
Lime putties used and their mineralogical composition.[a]

Lime putty	LP3[b]	LP12[b]	LP24[b]	LP36[b]	LP48	LP66
Aging time (months)	3	12	24	36	48	66
Brucite (wt%)	0.81	1.35	1.45	1.62	2.50	2.60
Portlandite (wt%)	81.30	85.70	86.80	86.10	86.09	86.98
Calcite (wt%)	12.31	9.50	10.10	9.87	10.60	10.49
Total composition (wt%)	94.42	96.55	98.35	97.59	99.20	100.07

[a] The mineralogical composition of the lyophilized samples was determined using thermo-gravimetric analysis (TGA).
[b] These lime putties contain small amounts of undetermined CaO and MgO, respectively.

In agreement with the results of the intruded volume mercury, the BET surface area slightly increases for the samples aged in the 3–48 months range, as reported in Table 3, whereas the sample aged for 66 months shows a certain increase, which perfectly agrees with the corresponding higher cumulative intruded volume mercury.

Particle size distributions of slaked lime putties, measured by static laser light scattering method are reported in Fig. 3 as volume frequency of particles versus particle diameter. In agreement with the wide pore size distributions results, each lime putty shows different classes of particle sizes. The shortest aged LP3 sample shows different classes of particle sizes in a relatively narrow 1–50 μm range of particle diameter. The more aged LP12 is characterized by a broader distribution of particle diameter in the range 0.3–200 μm , involving the formation of both larger and smaller portlandite particles or recrystallization of smaller ones. On further aging (LP24 sample), the broad particles size distribution persists and smaller particles of about 0.1 μm are also present. The longest-month-slaking lime putty LP66 is also characterized by various classes of particle size with a significant shift towards intermediate particle sizes.

It must be pointed out that the broader the distribution, the more the disparity produced between the volume frequency of large and small particles.

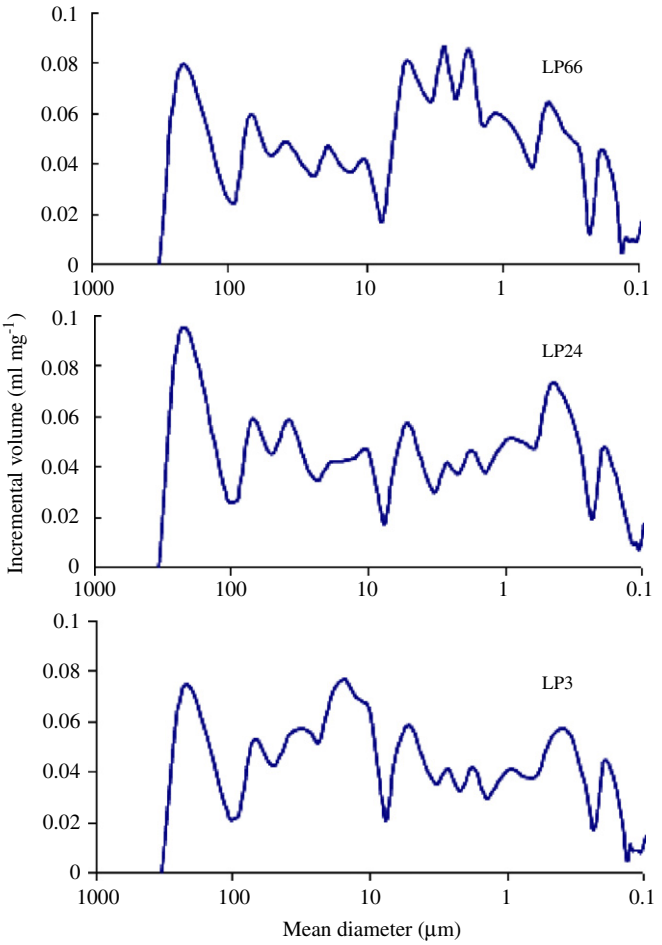

Fig. 2. Pore size distribution of LP3, LP24 and LP66 samples.

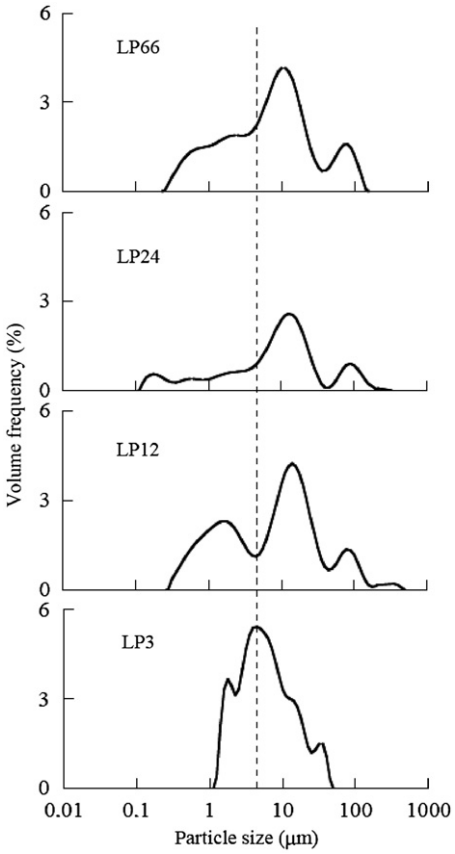

Fig. 3. Particle size distribution in terms of volume frequency of the lime putties slaked at increasing times.

Table 3
Surface area of lime putties aged for increasing time.

Lime putty	LP3	LP12	LP24	LP36	LP48	LP66
Surface area (m^2/g)	20.8	20.1	21.1	21.6	22.2	25.7

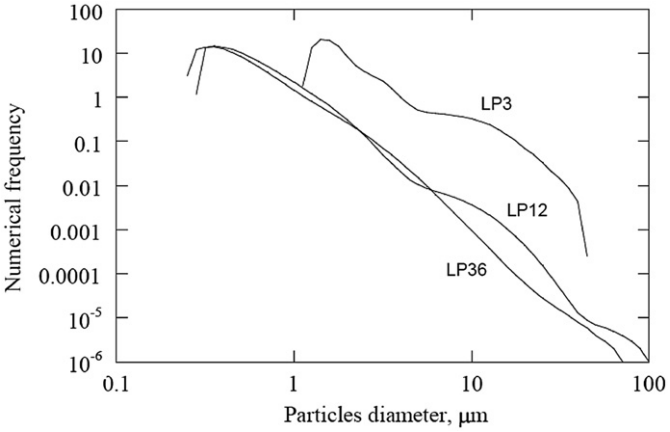

Fig. 4. Numerical frequency of particles versus particle diameter in putty samples aged at 3, 12 and 36 months.

Fig. 4 shows the numerical frequency of particles versus particle diameter for some samples listed in Fig. 3. The broader particles size distribution upon aging is confirmed, but the smaller particles are prevalent towards larger ones.

From the particle size distribution of each sample aged at various times, the average particles diameter has been calculated and reported in Fig. 5 assuming the particles to be spherical and adopting the volume weighted mean (curve *a*) or the surface weighted mean (curve *b*). Nevertheless for the different calculated diameters, attributable to the anisotropy of the portlandite crystals, an agreement in their behaviours can be seen. The average particles size increases upon aging and then decreases with a maximum at about 36 months.

On the contrary the water retention of the lime putties shows a minimum upon aging. It diminishes, in fact, from $64 \pm 0.5\%$ to $52 \pm 0.5\%$ for the lime putties slaked up to 24–36 months (Fig. 6) followed by an increase up to $60 \pm 0.5\%$ at 66-month slaking times. Consequently, an inverse ratio results between the average particles size and water retention.

By comparing the less-aged LP3 sample (SEM micrographs a and b of Fig. 7) with the most aged LP66 one (micrographs c–f of Fig. 7), it is confirmed that portlandite crystals undergo change in both shape and size upon aging [10]. Prisms or rounded particles (micrography a) and large hexagonal portlandite crystals (micrograph b) can be observed in the LP3 sample. The conspicuous shape change of the long aging lime putty (LP66) appears in micrography c, showing several and well developed hexagonal portlandite crystals, whereas micrography d shows some of these crystals with corroded edges. The LP66 sample is also characterized by the presence of numerous submicrometer platelike crystals on the surface and, in particular, on the periphery of the pre-existing portlandite crystals (micrography e). The long aging time favours aggregation of large and thin

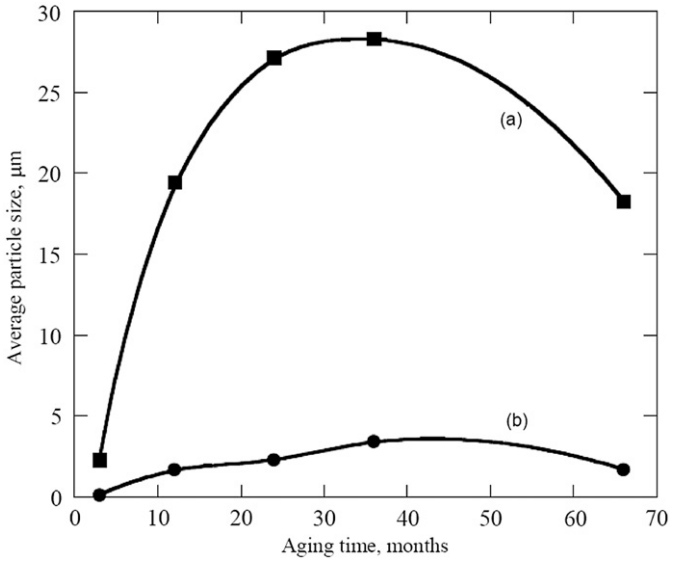

Fig. 5. Average particle diameter of the lime putties slaked at increasing times. Calculated assuming the particles to be spherical and adopting the volume weighted mean (a) or the surface weighted mean (b).

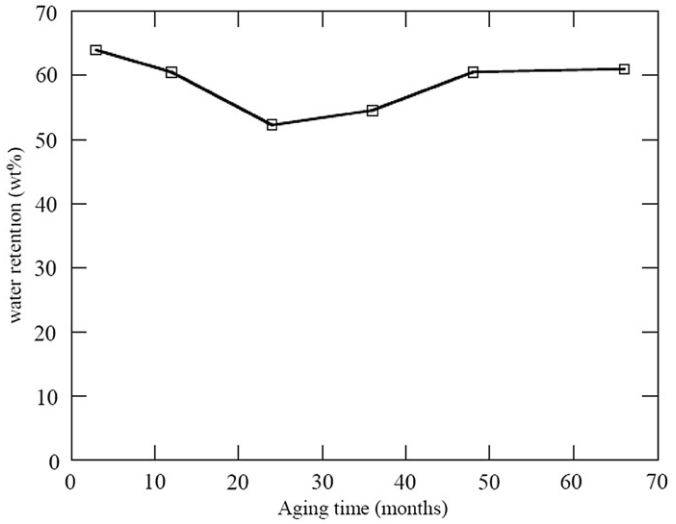

Fig. 6. Water retention content of the lime putties slaked at increasing times.

platelike crystals with the formation of numerous rose-like crystal habitus (micrography f).

4. Discussion

The microstructure evolution of lime putty upon aging reported in the literature claims two conflicting models. One theory associates the variation of both the size and the shape of portlandite crystals to the so-called "Ostwald ripening" [2,12,18], i.e. development of the larger crystals at the expense of the smaller ones. However, just the opposite has been frequently observed: the smaller portlandite crystals grow at the expense of the larger ones [11,19,20]. This last model is also based upon differences in solubility between {0 0 0 1} basal pinacoid faces and {1 0 $\bar{1}$ 0}, {1 0 $\bar{1}$ 1} prism faces responsible for a heterogeneous secondary nucleation with the formation of nanometer-scale portlandite crystals. Such differences in solubility are caused by surface energy (γ) difference between {0 0 0 1} basal pinacoid faces and {1 0 $\bar{1}$ 0}, {1 0 $\bar{1}$ 1} prism faces being γ_{0001} lower than both $\gamma_{10\bar{1}0}$ and $\gamma_{10\bar{1}0}$, respectively [21]. The attainment of the lowest total surface energy must be the driving force in promoting the continuous evolution upon aging of portlandite microstructure in terms of shape and size. Such evolution must be in accordance with both the "Ostwald ripening" [12] and the Wulff shape [22] concerning the crystal shape possessing the lowest surface energy for a fixed volume.

The development of small platelike portlandite crystals at the expense of the larger prism crystals appears thermodynamically unfavoredable [11]. Such a change may be considered as the result of the cutting of a prismatic crystal in the *c*-axis with the formation of separated thin plates of portlandite as shown in the schematic illustration of Fig. 8. The total surface energies per volume of the single prism crystal $\Gamma t_{(sp)}$ and of the corresponding thin plates $\Gamma t_{(tp)}$ are

$$\Gamma t_{(sp)} = S_{pr}\gamma_{pr} + S_{pi}\gamma_{pi} \quad \text{(single prism)}$$

$$\Gamma t_{(tp)} = S_{pr}\gamma_{pr} + S'_{pi}\gamma_{pi} \quad \text{(platelike crystals)}$$

where S_{pr}, S_{pi}, S'_{pi} are the surfaces of the prism faces, the surfaces of the basal pinacoid faces and γ_{pr} γ_{pi} the surface energy of prism faces and basal pinacoid faces, respectively. The shape change of Fig. 8 involves only a significant variation in the surface of the pinacoid faces changing from S_{pi} to the higher value S'_{pi}, so involving $\Gamma t_{(tp)} > \Gamma t_{(sp)}$. This result demonstrates that the formation of the small platelike portlandite crystals at the expense of the large prismatic crystal is thermodynamically unfavorable.

A possible and thermodynamically favorable portlandite evolution appears in the schematic illustration of Fig. 9. In this case the formation of large platelike crystals of portlandite with well developed {0 0 0 1} faces at the expense of smaller prismatic crystals (Ostwald ripening) involves a conspicuous increase of S_{pi} and a drastic diminution of S_{pr}. According to Ref. [11], being $\gamma_{pi} < \gamma_{pr}$, $\Gamma t_{(tp)}$ of the large hexagonal platelike crystal is lower than $\Gamma t_{(pr)}$.of the prism crystals. The frequent presence of large hexagonal platelike crystals, detected by SEM micrographs, in the less aged LP3 sample justifies this model. The nucleation secondary crystallization of submicrometer platelike portlandite crystals appears mainly as a consequence of the different solubility between prism faces and pinacoid faces connected to the large hexagonal platelike crystals. Secondary nucleation and crystallization of calcium hydroxide from aqueous solution was also found to occur in the presence of large seeds of $Ca(OH)_2$ [19].

If prevalent small plates would crystallize at the expense of the larger ones, a noticeable change in the BET surface area of the lime putty upon aging must be expected, but only a small increase has been detected in the 3–48 months range of aging as reported in Table 3. A certain increase has been detected for the longest aged sample LP66. To explain such negligible increases, several features must be taken into account for the evolution of the portlandite particles: the variation of the surface area/volume aspect ratio, the variation of the height to length aspect ratio [13] and the contemporaneous formation of both larger and smaller portlandite crystals.

The "corroded" edges frequently observed of large platelike crystals confirm the preferential dissolution of prism faces determining supersaturation followed by secondary nucleation–crystallization of submicrometer portlandite particles. The solubility differences between these small particles and larger ones [21] favour the formation of new large platelike crystals, which can aggregate on the pre-existing ones, thus justifying the presence of numerous aggregates as rose-like crystal habits. Such

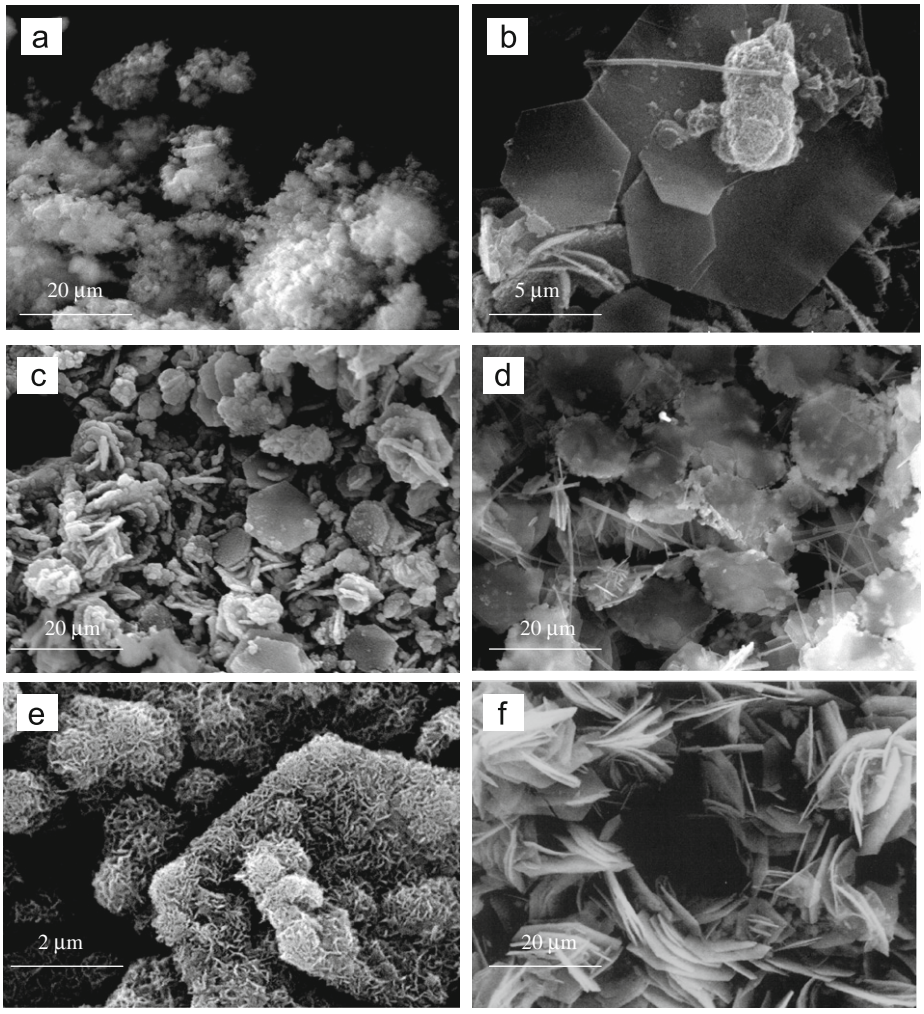

Fig. 7. SEM micrographs of LP3 (a, b) and LP66 samples (c, d, e, f).

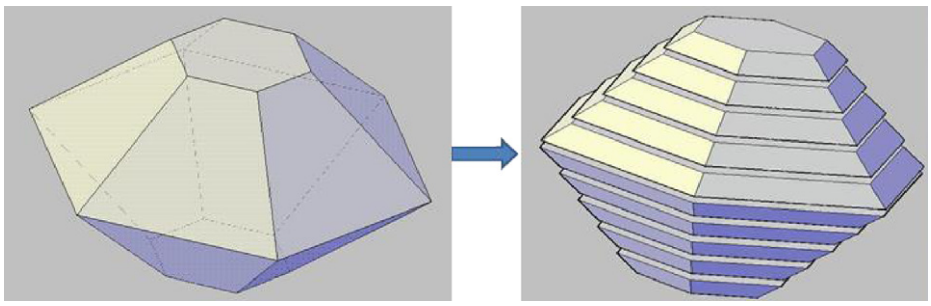

Fig. 8. Schematic illustration of a single prism portlandite crystal evolving towards smaller platelike crystals.

aggregated particle network can be related to the attraction between oppositely charged faces and edges.

The proposed mechanism justifies the continuous evolution of the microstructure of lime putty upon aging after many years of aging, thus involving a continuous dissolution and recrystallization of portlandite.

5. Conclusions

The attainment of the lowest total surface energy appears to be the driving force in promoting the continuous evolution upon aging of portlandite microstructure in terms of shape and size.

Nevertheless the important shape change from prism to platelike crystals, the sole reduction of the particles sizes upon aging in which the smaller portlandite crystals grow to the expense of the larger ones is not favorable for the diminution of the total surface energy. This diminution requires also the growth of large portlandite crystals as detected by SLS and SEM results. The nucleation and secondary crystallization of numerous submicrometer platelike crystals is a consequence of the anisotropy of such large crystals, which emphasizes the difference in the solubility between pinacoid faces and prism ones. The secondary crystallization of the submicrometer portlandite particles appears to be responsible for the continuous evolution of lime putty upon aging.

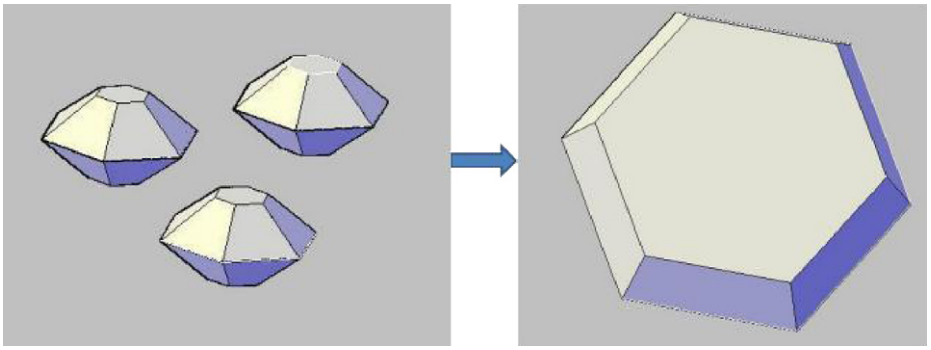

Fig. 9. Schematic illustration of prismatic portlandite crystals evolving towards a single large hexagonal crystal.

The continuous change in the morphology of portlandite also affects the content of water retention, which is one of the features affecting the workability of the lime putty. An inverse ratio between the amount of water retention and the corresponding average particle size has been detected. For the shortest aged LP3 sample, nevertheless its highest water retention content, due to the lowest average particle size, a low plasticity and workability must be expected due to the reduced shape change from prismatic to platelike crystals; consequently, this shape change is decisive for the optimization of putty workability.

It is confirmed that the better quality of lime putties increases with the extended exposure of quicklime to water. As established by an ancient Roman law, an aging time longer than 36 months is necessary. A surprising fact is that this aging time corresponds to the minimum in the water retention content and to the maximum in the average particles sizes as has been detected.

Acknowledgement

The authors wish to thank Sebastiana Dal Vecchio and Alberto Colantuono for providing lyophilisation of samples and SEM micrographs.

References

[1] J. Ashurst, Mortars for stones buildings, in: J. Ashurst, F.G. Dimes (Eds.), Conservation of Building and Decorative Arts, vol. 2, Butterworths, London, UK, 1990, pp. 78–96.
[2] G. Torraca, in: Porous Building Materials, 3rd ed., International Centre for the Study of the Preservation and Restoration of Cultural Property, Rome, Italy, 1988.
[3] W.D. Kingery, A role for ceramic materials science in art, history and archaeologyJ. Mater. Ed. 9 (6) (1987).
[4] J.M. Teutonico, I. McCaig, C. Burns, J. Ashurst, The smeaton project: factors affecting the properties of lime-based mortars, Assoc. Preserv. Technol. Bull. 25 (1994) 32–49.
[5] G. Biscontin, M. Piana, and G. Riva, Research on lime and intonacoes of the historical venetian architecture, in: Proceedings of the Symposium on Mortars, Cements, and Grouts Used in the Conservation of Hystoric Buildings. International Centre for the Study of the Preservation and Restoration of Cultural Property, Rome, Italy, 1981, pp. 359–374.
[6] National Lime Association, Specification for lime and its uses for plastering, stucco, unit masonry and concrete, Lath Plaster 9 (1996) 1–16.
[7] T. Ritchie, Study of efflorescence produced on ceramics wicks by masonry mortars, J. Am. Ceram. Soc. 38 (1955) 362–366.
[8] G. Plinio II, Naturalis Historia, libro V, G. Einaudi, Torino, Italy, 1988, pp. 709–711.
[9] Vitruvio, De Architettura, libro VII,G. Einaudi, Torino, Italy,1997, p. 1033.
[10] R.S. Boynton, in: Chemistry and Technology of Lime and Limestone, 2nd ed., Wiley, New York, 1980.
[11] C. Rodriguez-Navarro, E. Hansen, W.S. Ginell, Calcium hydroxide crystals evolution upon aging of lime putty, J. Am. Ceram. Soc. 81 (11) (1998) 3032–3034.
[12] W. Ostwald, Über die vermeintliche isomeric des roten und gelben quecksilberoxyds under die oberflächenspannung fester körper, Z. Phys. Chem. 34 (1900) 495–503.
[13] O. Cazalla, C. Rodriguez-Navarro, E. Sebastian, G. Coltrone, Aging of lime putty: effects on traditional lime mortar carbonation, J. Am. Ceram. Soc. 83 (5) (2000) 1070–1076.
[14] C. Atzeni, A. Farci, D. Floris, P. Meloni, Effect of aging on rheological properties of lime putty, J. Am. Ceram. Soc. 87 (9) (2004) 1764–1766.
[15] A. Maropoulou, A. Bakolas, E. Aggelakopoulou, The effects of limestone characteristics and calcination temperature on the reactivity of quicklime, Cem. Conc. Res. 31 (4) (2001) 633–639.
[16] D.T. Beruto, F. Barberis, R. Botter, Calcium carbonate binding mechanism in the setting of calcium and calcium–magnesium putty lime, J. Cult. Heritage 6 (3) (2005) 253–260.
[17] F.C. Meldrum, S.T. Hyde, Morphological influence of magnesium and organic additives on the precipitation of calcite, J. Cryst. Growth 231 (2001) 544–558.
[18] H.H. Bache, G.M. Dorn, P. Nepper-Christensen, J. Nielsen, Morphology of calcium hydroxide in cement pastes, in: Proceedings of the Symposium on the Structure of Portland Cement Paste and Concrete, Special Report no. 90, 1966, pp.154–174.
[19] B. Tomazic, R. Mohanty, M. Tadros, J. Estrin, Crystallization of calcium hydroxide from aqueous solution: ii. Observation of growth, morphology and secondary nucleation, J. Cryst. Growth 75 (1986) 339–347.
[20] D.E. Giles, I.M. Ritchie, B.A. Xu, The kinetics of dissolution of slaked lime, Hydrometallurgy 32 (1993) 119–128.
[21] A.W. Adamson, in: Physical Chemistry of Surface, 5th ed., Wiley, New York, 1990.
[22] G. Wulff, Zur frage geschwindigkeit des wachsthums und der auflösung der kristallflachen, Z. Kryst. Mineral 34 (1901) 449–530.